ISOCAM observations of the L1551 star formation region *,**

M. Gålfalk[1], G. Olofsson[1], A.A. Kaas[2], S. Olofsson[1], S. Bontemps[3], L. Nordh[4], A. Abergel[5], P. André[6], F. Boulanger[5], M. Burgdorf[13], M.M. Casali[8], C.J. Cesarsky[6], J. Davies[9], E. Falgarone[10], T. Montmerle[6], M. Perault[10], P. Persi[11], T. Prusti[7], J.L. Puget[5], and F. Sibille[12]

[1] Stockholm Observatory, Sweden
[2] Nordic Optical Telescope, Canary Islands, Spain
[3] Observatoire de Bordeaux, Floirac, France
[4] SNSB, Box 4006, 171 04 Solna, Sweden
[5] IAS, Université Paris XI, Orsay, France
[6] Service d'Astrophysique, CEA Saclay, Gif-sur-Yvette, France
[7] ISO Data Centre, ESA Astrophysics Division, Villafranca del Castillo, Spain
[8] Royal Observatory, Blackford Hill, Edinburgh, UK
[9] Joint Astronomy Center, Hawaii
[10] ENS Radioastronomie, Paris, France
[11] IAS, CNR, Rome, Italy
[12] Observatoire de Lyon, France
[13] SIRTF Science Center, California Institute of Technology, 220-6, Pasadena, CA 91125, USA

Abstract.
The results of a deep mid-IR ISOCAM survey of the L1551 dark molecular cloud are presented. The aim of this survey is a search for new YSO (Young Stellar Object) candidates, using two broad-band filters centred at 6.7 and 14.3 μm. Although two regions close to the centre of L1551 had to be avoided due to saturation problems, 96 sources were detected in total (76 sources at 6.7 μm and 44 sources at 14.3 μm). Using the 24 sources detected in both filters, 14 were found to have intrinsic mid-IR excess at 14.3 μm and were therefore classified as YSO candidates. Using additional observations in *B*, *V*, *I*, *J*, *H* and *K* obtained from the ground, most candidates detected at these wavelengths were confirmed to have mid-IR excess at 6.7 μm as well, and three additional YSO candidates were found. Prior to this survey only three YSOs were known in the observed region (avoiding L1551 IRS 5/NE and HL/XZ Tau). This survey reveals 15 new YSO candidates, although several of these are uncertain due to their extended nature either in the mid-IR or in the optical/near-IR observations. Two of the sources with mid-IR excess are previously known YSOs, one is a brown dwarf (MHO 5) and the other is the well known T Tauri star HH 30, consisting of an outflow and an optically thick disk seen edge on.

Key words. stars: formation – stars: low-mass, brown dwarfs – stars: pre-main sequence – stars: late-type – infrared: stars

1. Introduction

The L1551 dark molecular cloud (Lynds 1962) is one of the nearest and therefore most studied regions of low-mass star formation. It is part of the Taurus-Auriga molecular cloud complex and the distance to its leading edge has been measured to

be 140±10 pc (Kenyon et al. 1994). It shows the usual signs of recent star formation: pre-main-sequence stars (Briceño et al. 1998), Herbig-Haro objects (Devine et al. 1999), reflection nebulosity and an extraordinary bipolar outflow (Snell et al. 1980; Rainey et al. 1987; Fridlund & White 1989a, 1989b; Parker et al. 1991) that has become a prime example of this outflow type. This outflow emanates from the IR-source L1551 IRS 5 (Strom et al. 1976; White et al. 2000; Osorio et al. 2003), a deeply embedded Young Stellar Object (YSO) found to be a binary (Looney et al. 1997). Another well known IR-source with a molecular outflow is L1551 NE, a binary (Moriarty-Schieven et al. 2000) or even triple (Reipurth 2000) YSO, discovered with the IRAS satellite (Emerson et al. 1984). Among the numerous Herbig-Haro objects of the L1551 region, the very compact HH 30 is a well known YSO with a disk and

jets that have been imaged by the HST (Burrows et al. 1996). During the ISO (Infrared Space Observatory) mission several nearby dark clouds were surveyed. In this paper we present mid-IR observations of the L1551 region using ISOCAM onboard the ISO-satellite.

The low-mass end of the IMF (Initial Mass Function) is a key objective when investigating star formation, especially for stars lying in the brown dwarf region (below the Hydrogen burning limit of 0.08 $M_\odot$) where the IMF is not well known. Since L1551 is a nearby star formation cloud, located far away from the crowded Galactic plane ($b = -20°$), it should be possible to detect such low-mass stars using ISOCAM. YSO-candidates can generally be found from the ISOCAM data by searching for sources with mid-IR excess, due to heated circumstellar dust. These mid-IR observations have high sensitivity and high spatial resolution, and are therefore suitable for finding and classifying YSOs, as shown for other clouds (Olofsson et al. 1999; Kaas et al. 1999; Persi et al. 2000; Bontemps et al. 2001).

The young stellar population in L1551 has previously been surveyed using several methods: X-ray mapping (Carkner et al. 1996; Favata et al. 2003); Optical and near-IR mapping (e.g. Briceño et al. 1998); Optical spectra (Gomez et al. 1992) and Hα surveys (e.g. Garnavich et al. 1992). However, no mid-IR survey as sensitive as this ISOCAM survey (down to ~0.5 mJy) had previously been done in L1551.

Lada & Wilking (1984) used observations between 1 and 20 μm to plot the mid-IR Spectral Energy Distribution (SED) of embedded sources in the Ophiuchi dark molecular cloud and found that the population could be divided into three morphological classes. Later (Lada 1987) this YSO classification scheme (Class I–III) was made more quantitative by introducing the spectral index α and approximate limits for the classes. A Class 0 was then introduced (André et al. 1993) and the classification limits were also revised (André & Montmerle 1994). These four YSO classes are defined in a morphological order with Class 0 sources being protostars at the beginning of the main accretion phase, deeply embedded in massive, cold circumstellar envelopes. Class I sources are more evolved and Class II YSOs are T Tauri stars with optically thick IR circumstellar disks. Class III YSOs represent weak line T Tauri stars with at most optically thin disks, they are therefore hard or impossible to detect using mid-IR excess due to their resemblance to field stars. Therefore, using ISOCAM mid-IR observations, mainly classes I & II are detected since Class 0 objects peak in the far-IR spectral region and are probably too weak in the mid-IR to be detected by ISOCAM. The evolution from Class 0 to Class III has classically been assumed to be smooth and gradual, and while this might be the case for isolated young stars it has recently been suggested (Reipurth 2000) that abrupt class transitions can occur in multiple systems due to violent interactions between its members. Massive and quick disk truncation combined with the possible ejection of light cluster members could then produce highly increased outflow activity as well as transitions from Class 0 or I objects to visible T Tauri stars.

2. Observations and data reductions

Six regions (total area 0.122 sq.deg.) were observed 26–27 September 1997 with ISOCAM, avoiding the mid-IR bright regions around IRS 5/NE and HL/XZ Tau due to saturation problems. Two mid-IR filters were used with the LW (Long Wavelength) detector, LW2 (6.7 μm) and LW3 (14.3 μm). For all images, the PFOV is 6″/pixel and the integration time was 2.1 s for each transmitted frame (32 × 32 pixels). During the reduction, around 19 frames were combined at each frame-position to form images with a temporal history. Also, overlaps of half a frame in both equatorial directions gives the much needed spatial redundancy as well as additional temporal history. A total of 286 images were used to put together the 6.7 and 14.3 μm mosaics. Unfortunately the LW detector had a dead column (No 24), which however could be covered by using overlapping images for most parts of the final L1551 mosaic. Only at some parts close to the southern limit of the mosaic (due to a spacecraft roll angle of 83°) and close to IRS 5/NE there is missing information, but not more than about 0.3 % of the mapped region. Also, the photometry of sources one pixel from the dead column and at the mosaic edges is unreliable.

For the data reduction, we used the CIA V4.0 package (Ott et al. 1997; Delaney et al. 2000) and the SLICE package (Simple & Light ISOCAM Calibration Environment) accessed from inside CIA. The CIA reduction steps consisted of (in order): Extracting useful observations, dark correction (Vilspa dark model, Biviano et al. 2000), glitch removal (multiresolution median transform, Starck et al. 1996), short transient correction (Fouks-Schubert model, Coulais & Abergel 2000), flatfielding (constant median flatfield from observations). The data were then processed further using SLICE's long-term transient and variable flatfield algorithms (Miville-Deschnes et al. 1999). Finally the frames were projected into six raster maps for point source detection and photometry. Each detected point source was traced back to its corresponding original frames for temporal and spatial verification (in order to exclude remaining artefacts). For the aperture photometry, the point spread function was used to correct for flux outside the aperture. In total 96 sources were detected with photometry possible for 76 sources at 6.7 μm and 44 sources at 14.3 μm. Regarding photometric comparison, 24 sources had photometry in both filters and could therefore be classified using a colour diagram. A correlation between the two filters is reasonable to assume for a source separation of less than about one pixel (6″), however, to allow for correlations in nebulous regions a limit of 8″5 has been used. The mean separation of all correlated sources is however ~ 2″5.

Even though the integration time was 2.1 s for each frame and there are about 19 frames for each image, the total exposure time for a pixel in the mosaic varies between 40 s and 160 s due to the half frame overlaps in both RA and Dec which makes the total number of frame-pixels available for a mosaic pixel vary by a factor of 1 to 4. Therefore, it is expected that the faintest sources will generally be detected (half a frame, 16 pixels) away from the mosaic edges. From mean uncertainty calculations of all detected ISOCAM sources in L1551, photometric uncertainties are estimated to be (1σ) 0.4 mJy at 6.7 μm
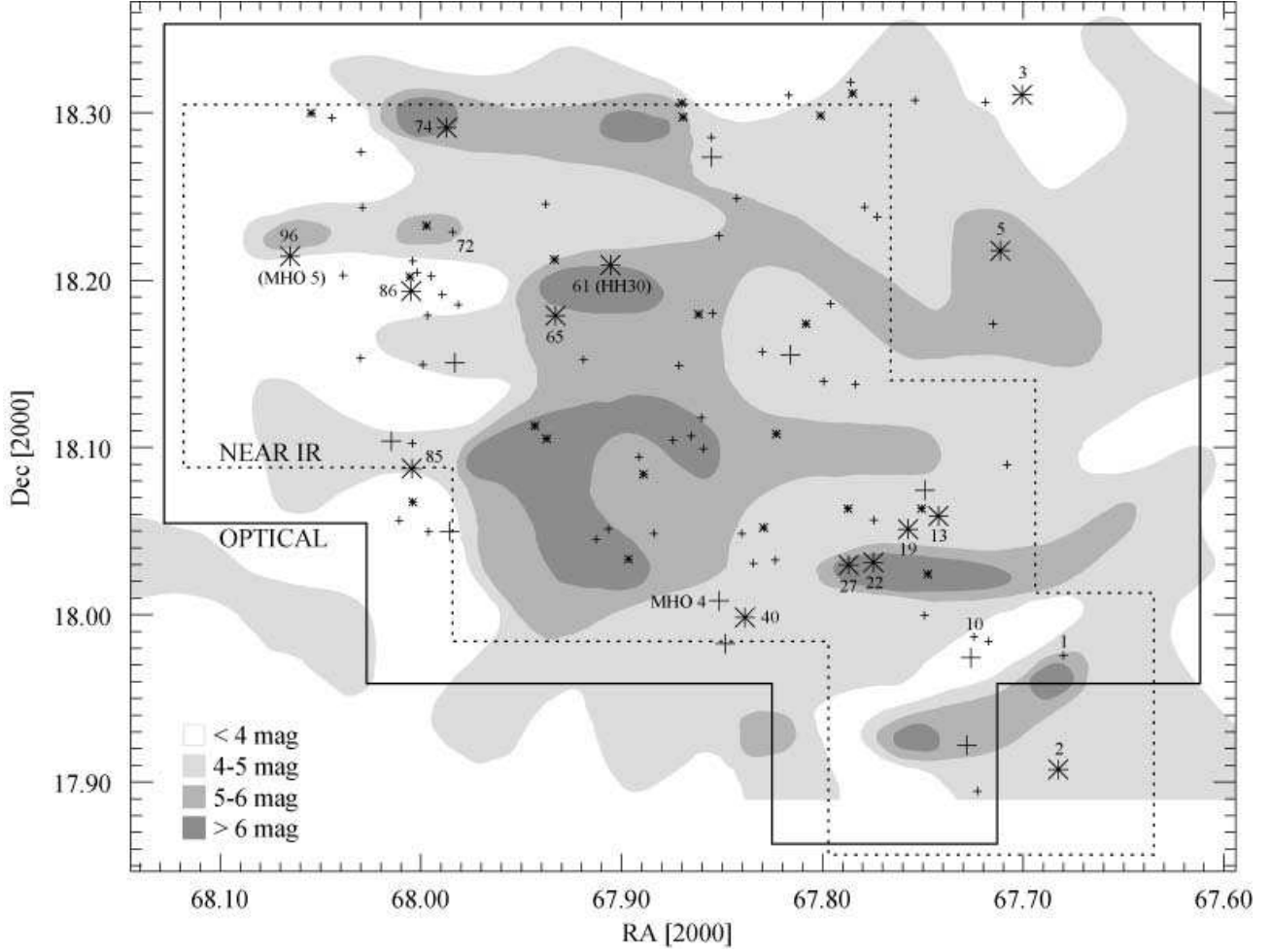
Fig. 1. The spatial distribution of all sources detected with ISOCAM, where the large asterisks and plus signs represent 'red' and 'blue' sources respectively in the $m_{6.7} - m_{14.3}$ colour (see Table 2). The small asterisks and plus signs represent sources only detected at $14.3 \, \mu m$ and $6.7 \, \mu m$ respectively. The region observed at optical wavelengths (B, V and I) is marked by a solid line while the region observed in the near-IR (K) is marked by a dotted line. The contours indicate the visual extinction in magnitude steps (Minn 1991).

and $0.5 \, mJy$ at $14.3 \, \mu m$ which also approximately represent the detection limits, however as faint sources as these are only detected in low nebulosity regions without artefacts and by using variable flatfielding. On the other hand the surveyed region is not completely mapped down to the 1σ level, since it is possible that even sources brighter than 3σ ($1.2 \, mJy$ and $1.5 \, mJy$ respectively) may have been unnoticed due to varying nebulosity, glitches, memory effects, uncovered dead columns and source confusion close to very bright sources. As for the positional accuracy, by using the 19 LW2 sources also seen in the USNO-A2.0 (Monet) catalogue the uncertainties have been estimated to 0.13 s in right ascension and 3″3 in declination.

In order to convert mJy fluxes into $6.7 \, \mu m$ and $14.3 \, \mu m$ magnitudes, we used the following relations:

$$m_{6.7} = 12.30 - 2.5 \log_{10} F_{6.7}$$
$$m_{14.3} = 10.69 - 2.5 \log_{10} F_{14.3}$$

Additional observations were made in Hα and the B, V, I and K bands using the 2.56 m NOT telescope in La Palma, Canary Islands, Spain. The K band observations were obtained

23, 24 and 27 August 1996 using the Arcetri NICMOS3 camera, ARNICA, a near-IR (1–2.5 μm) 256 × 256 pixel HgCdTe array yielding a 2′×2′ FOV. The observed region covered about the same region as the ISOCAM mid-IR observations and were divided into four mosaics: NN (4 × 4 fields), N (11 × 7 fields), S (9×5 fields) and SS (5×5 fields). The overlap was 0″5 in both equatorial directions for all fields. Photometry was done on the individual fields down to the limiting magnitude of $K \sim 17.5$. There were actually 60 co-added images of 1 s each in order not to saturate too many sources, giving a total exposure time of 60 s for each field.

The B, V, and I observations were carried out on 1 and 3 December 2001 using the ALFOSC instrument (Andalucia Faint Object Spectrograph and Camera) mounted on the 2.56 m NOT telescope. This instrument has a 2048 × 2048 pixel CCD chip and at a PFOV of 0″188/pixel it has a FOV of about 6′4 × 6′4. We originally set out to do a 5 × 5 field mosaic of the entire ISOCAM region with an overlap of 45″, however, due to bad weather on 3 out of the 5 allocated nights we observed the 20 most important frames in the mosaic (regarding ISOCAM
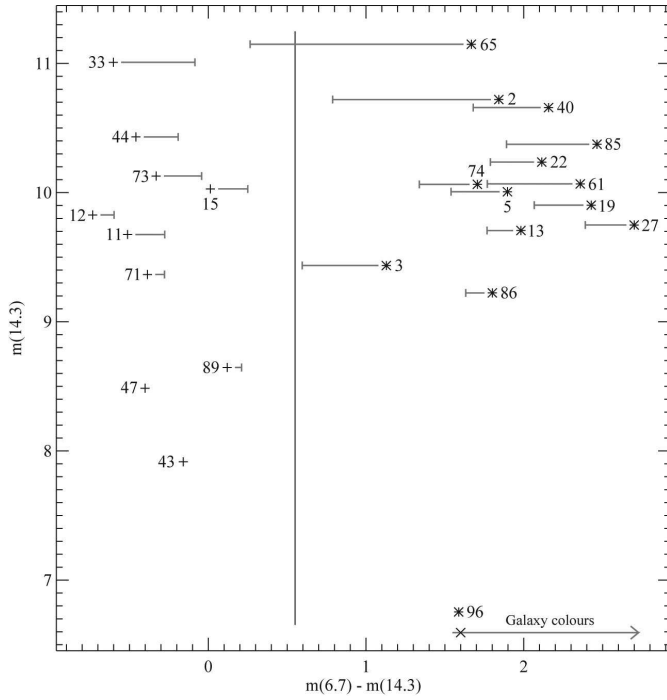
Fig. 2. This mid-IR colour/magnitude plot clearly shows two populations (separated by a dividing line), one with a colour index close to zero and one 'red' population with $14.3\,\mu$m excess. The arrow indicates expected galaxy colours for ISOCAM observations.
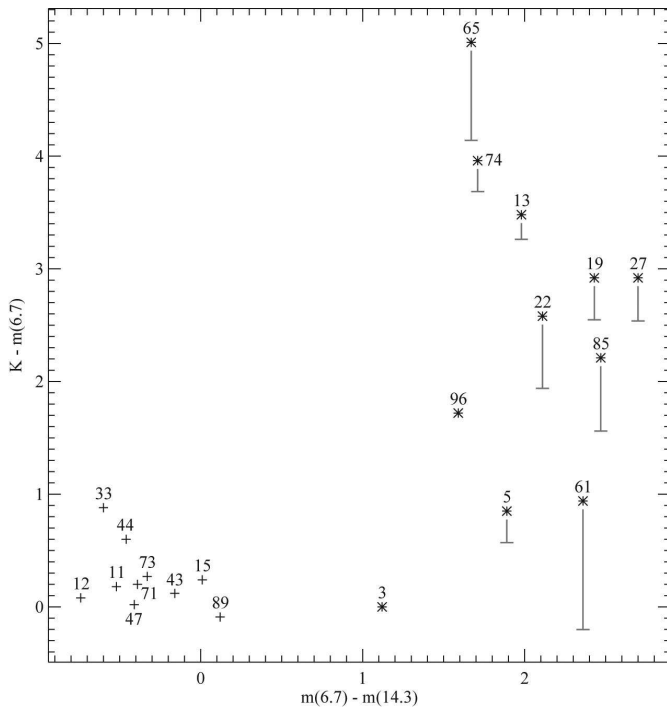

Fig. 3. In this colour/colour diagram for all ISOCAM sources with available K_S, $6.7\,\mu$m and $14.3\,\mu$m magnitudes it is clearly seen that most 'red' (asterisks) and 'blue' (plus signs) sources in the $m_{6.7} - m_{14.3}$ index remain 'red' and 'blue' separated in the $K - m_{6.7}$ colour index.
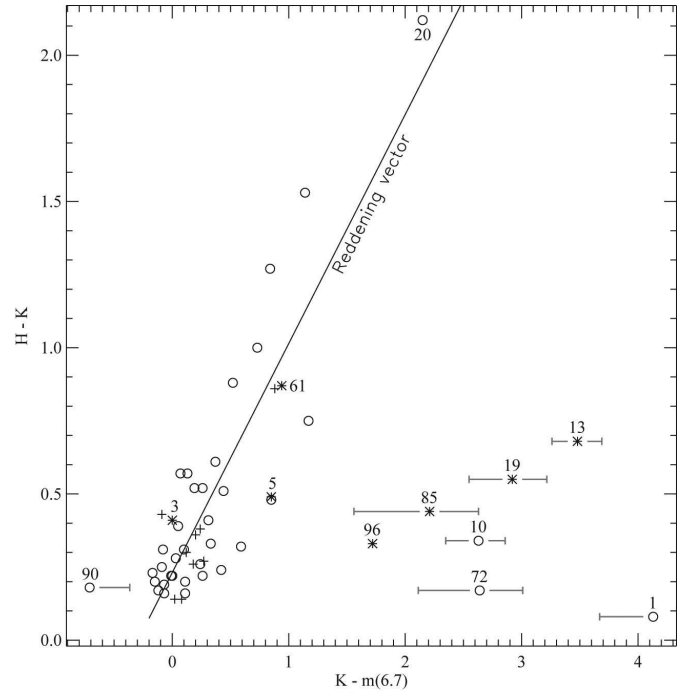

Fig. 4. In this colour/colour diagram for ISOCAM sources with H and K magnitudes, ISO-L1551-1, 10 and 72 are suggested to be YSO candidates due to excess in the $K - m_{6.7}$ colour index. Symbols are the same as in Fig. 2 except that circles represent sources not detected at $14.3\,\mu$m. The interstellar reddening vector was calculated by fitting a line to the blue and previous unclassified sources (circles).

source coverage). We used the following NOT-filters and exposure times: B#74 (440 nm, 420 s), V#75 (530 nm, 300 s) and i#12 (797 nm, 180 s and 10 s) yielding detection limits of about 22.5, 22.5 and 22.0 mag. respectively. The seeing was typically $0''9$ for both nights. Finally, the Hα observations were also observed with ALFOSC on the NOT telescope. Two images were obtained on the night of 22–23 October 2001 using an exposure time of 1200 s. These were later put together into a mosaic.

3. Results

Figure 1 illustrates the spatial distribution of all sources detected with ISOCAM, where the visual extinction in magnitude steps is used to indicate the extent of the L1551 dark molecular cloud (contours adopted from Minn 1991). The distribution appears to be homogeneous, i.e. no apparent correlation between ISOCAM source positions and visual extinction. The B, V, I and K observations cover roughly the same region as the ISOCAM mosaic, but as the figure shows, one source (ISO-L1551-2) is not included in the optical observations and 15 sources were missed in the near-IR. However, the 2MASS point source catalogue has been used to obtain near-IR (J, H and K_S) photometry in the whole ISOCAM region.

The final ISOCAM $6.7\,\mu$m mosaic is presented in Fig. 6 with all $6.7\,\mu$m sources circled. As mentioned previously, two regions (close to IRS5/NE and HL/XZ Tau) were avoided due to saturation issues.

In Table 2, all detected ISOCAM sources are presented along with optical and near-IR photometry. Parenthesis are used to indicate very uncertain sources, where no optical or near-IR counterpart has been found and where typically, there is only one overlap available in the 6.7 or 14.3 μm mid-IR data. Also, bold source numbers indicate sources with an ISOCAM mid-IR excess in the $m_{6.7} - m_{14.3}$ index (i.e. YSO candidates). As stated before, the faintest sources should be detected in regions with the most overlaps. In fact, almost all sources with a LW2 or LW3 flux below 1 mJy are located in regions where four image-pixels (4 × 19 frame-pixels) overlap, giving an exposure time of up to 160 s.

In the ISOCAM mid-IR colour/magnitude plot (Fig. 2), two populations ('red' and 'blue') can clearly be seen based on the $m_{6.7} - m_{14.3}$ colour index. These populations are well separated by a colour index gap larger than one magnitude. Sources with negligible uncertainties in the $m_{6.7} - m_{14.3}$ index, with respect to the red-blue dividing line, have no error bars in the plot. Generally, fainter sources at 14.3 μm have larger colour error bars, with ISO-L1551-65 being the most uncertain 'red' source in the plot (it is however confirmed as a red source in Fig. 3). ISO-L1551-3 has larger error bars than might be expected from its 14.3 μm magnitude, it has however only one overlap in the ISOCAM mosaics (making its temporal history quite uncertain) and is located close to a mosaic edge, making its sky background uncertainty larger as well.

Interstellar reddening in the $m_{6.7} - m_{14.3}$ colour index is small or not even present since 'blue' ISOCAM (background) sources are also seen in regions with quite large extinction (see Fig. 1), therefore sources without intrinsic 14.3 μm excess should be located close to 0 in the $m_{6.7} - m_{14.3}$ index. For the stars with near-IR photometry, the intrinsic and interstellar reddening effects can easily be separated in a colour/colour diagram using a reddening vector, which indicates the interstellar reddening in the two colours. A set of colour/colour diagrams using near-IR and mid-IR photometry are presented in Figures 3 and 4. The reddening vector in Fig. 4 was calculated by fitting a line to the blue and previously unclassified sources. There is no reddening line in Fig. 3 since this would be an almost vertical line due to the very small interstellar extinction in the $m_{6.7} - m_{14.3}$ colour. As can be seen from these figures, most sources with red $m_{6.7} - m_{14.3}$ colours are also red in the $K - m_{6.7}$ colour and the 'blue' sources remain 'blue'. Thus, these ISOCAM mid-IR excesses are confirmed as intrinsic. The $m_{6.7} - m_{14.3}$ red sources ISO-L1551-3 and 61 have no excess at 6.7 μm (see Fig. 4). ISO-L1551-61 is however the known YSO HH 30, consisting of an outflow and an optically thick disk seen edge on and ISO-L1551-3 is probably a Class III YSO and thus has a small excess (at 14.3 μm). We also note that three sources (ISO-L1551-1, 10 and 72), not detected at 14.3 μm, show intrinsic mid-IR excesses (at 6.7 μm). They are therefore added to our list of sources with mid-IR excesses (i.e. YSO candidates). The ISOCAM 'red' source ISO-L1551-2 could not be plotted in the colour/colour diagrams since the mid-IR photometry is very uncertain due to its proximity to an uncovered dead column in the 6.7 μm and 14.3 μm mosaics. However, since roughly the same relative flux is lost on the dead column for

both mid-IR filters, ISO-L1551-2 is still included as a YSO candidate.

In Table 1 we list all ISOCAM sources with mid-IR excess and which are therefore YSO candidates. Cross correlations with previous source names and YSO status are given. Using the SED indices $\alpha_{6.7-14.3}$ and $\alpha_{2.2-6.7}$ all YSO candidates have been classified into YSO classes I–III (mostly Class II). For the ISOCAM fluxes, the classical IR spectral index becomes:

$$\alpha_{6.7-14.3} = \frac{d \log(\lambda F_\lambda)}{d \log \lambda} = -\frac{d \log(\nu F_\nu)}{d \log \nu} = \frac{\log(F_{14.3}/F_{6.7})}{\log(14.3/6.7)} - 1$$

and for the K & 6.7 μm fluxes we similarly have:

$$\alpha_{2.2-6.7} = \frac{\log(F_{6.7}/F_{2.2})}{\log(6.7/2.2)} - 1$$

Classification limits (Class I–III) for both α indices have been assumed to be the same as in many previous ISOCAM studies (e.g. Kaas et al. 1999; Bontemps et al. 2001). For the ISOCAM spectral index, we thus have: Class I/II limit at $\alpha_{6.7-14.3} \sim 0$, Class II/III limit at $\alpha_{6.7-14.3} \sim -1.6$ and for no excess (simple photospheric blackbody emission) we have $\alpha_{6.7-14.3} \sim -3.0$. For the three YSO candidates without 14.3 μm flux, the classification was done using the $\alpha_{2.2-6.7}$ index. The total flux uncertainties for the YSO candidates in Table 1 were obtained by adding the spatial and temporal errors in quadrature. Temporal errors were estimated from frame photometry (in all overlaps) for each source position, spatial errors were calculated from the background sky variation close to each source (taking into account the aperture size used).

Of the 17 YSO candidates, only two (HH 30 and MHO 5) were previously known to be YSOs. There is a third previously known YSO (MHO 4, Briceño et al. 1998) in the ISOCAM region, however, for which we lack evidence of YSO status. It is detected at both 6.7 and 14.3 μm (ISO-L1551-44) but shows no mid-IR excess. This source has also been observed as an X-ray source (L1551 X15, Carkner et al. 1996). Some of the new YSO candidates in Table 1 are doubtful since they are either extended or lie close to a known Herbig-Haro object. Also, ISO-L1551-1 has an uncertain YSO status since it was not detected at 14.3 μm and its optical/near-IR counterpart is located more than 8″ from the ISOCAM position. ISO-L1551-2 is doubtful since it, as described above, lies partially on an uncovered dead column in both ISOCAM mosaics.

4. Discussion

Although the ISOCAM mid-IR ($m_{6.7} - m_{14.3}$) colour is efficient in separating field stars from YSO candidates, there are mainly three other types of objects that could 'contaminate' the survey and be mistaken for YSOs. These are: very 'red' field stars (AGB or M7III spectral types), galaxies and Herbig-Haro objects.

From the Wainscoat et al. (1992) model of the point source mid-IR sky, statistically there should be no AGB or M7III field stars in our field, these could otherwise be mistaken for YSOs due to their mid-IR brightness.

Table 1. Summary for ISOCAM sources with mid-IR excess (YSO candidates).

ISO-L1551	$F_{6.7}$ [mJy]	$F_{14.3}$ [mJy]	$F_{14.3}/F_{6.7}$	$\alpha_{6.7-14.3}$	YSO type[d]	Status	Comments
				New YSO candidates			
1	1.56 ± 0.47	—	—	+0.55[c]	Class II[c]	New	Mid-IR excess at 6.7 μm (S comp.)
2	0.79:	0.97:	1.24:	−0.72:	Class II ?	New	Partially on dead column
3	4.95 ± 0.68	3.18 ± 1.21	0.64	−1.58	Class II / III	New	
5	1.44 ± 0.33	1.88 ± 0.43	1.30	−0.65	Class II	New	
10	2.00 ± 0.45	—	—	−0.68[c]	Class II[c]	New	Mid-IR excess at 6.7 μm
13	1.76 ± 0.21	2.47 ± 0.38	1.41	−0.55	Class II	New	Extended + Close to GH 2[a]
19	0.97 ± 0.27	2.07 ± 0.43	2.12	−0.01	Class I / II	New	
22	0.95 ± 0.29	1.52 ± 0.40	1.59	−0.39	Class II	New	Extended
27	0.87 ± 0.23	2.38 ± 0.37	2.73	+0.32	Class I	New	Extended
40	0.62 ± 0.23	1.03 ± 0.28	1.66	−0.34	Class II	New	XMM-Newton-15, Favata et al. 2003
65	0.62 ± 0.25	0.66 ± 0.47	1.05	−0.93	Class II	New	VLA 21cm - 15[b]
72	0.87 ± 0.33	—	—	−0.68[c]	Class II[c]	New	Mid-IR excess at 6.7 μm
74	1.63 ± 0.33	1.78 ± 0.45	1.09	−0.88	Class II	New	Extended
85	0.61 ± 0.28	1.34 ± 0.43	2.20	+0.04	Class I / II	New	Double in optical (S comp. extended)
86	3.24 ± 0.38	3.86 ± 0.41	1.19	−0.77	Class II	New	Close to HH 262
				Previously known YSOs			
61	0.89 ± 0.58	1.77 ± 0.59	1.99	−0.09	Class I / II	HH 30	Circumstellar disk seen edge-on
96	38.34 ± 0.71	37.55 ± 0.62	0.98	−1.03	Class II	MHO 5	Spectral type M6 - M6.5

Note - Bold source numbers indicate YSO candidates based on mid-IR excess emission in the ISOCAM $m_{6.7} - m_{14.3}$ index

[a] Graham & Heyer 1990
[b] Giovanardi et al. 2000 - Could be an extragalactic triple radio source (Rodríguez & Cantó 1983)
[c] Spectral index $\alpha_{2.2-6.7}$ has been used
[d] As implied by $\alpha_{6.7-14.3}$, assuming that all candidates are YSOs

In Fig. 2, an arrow has been drawn indicating expected $m_{6.7} - m_{14.3}$ colours of galaxies. For a galaxy with no 14.3 μm excess (i.e. $F_{6.7} = F_{14.3}$) we expect a colour of $m_{6.7}-m_{14.3} \sim 1.6$ (marked with an x on the arrow). The arrow was adopted from ISOCAM observations of 46 non-saturated galaxies (Dale et al. 2000), including normal star-forming galaxies of many morphological types (Ellipticals, Lenticulars, early to late type Spirals, Irregular & Peculiar types). The bluest of these galaxies are located close to the 'no 14.3 μm excess mark' (Quiescent galaxies) while galaxies with higher star formation rates and 'red' morphological types are located further along the arrow. There is a probability of about 70 % for a randomly observed galaxy to be located within the colours of the arrow, while starburst galaxies may be located at much 'redder' colours. From the discussion above, it is clear that differentiation between YSOs and galaxies using only the $m_{6.7} - m_{14.3}$ colour is impossible. According to the ELAIS (European Large Area ISO Survey) ISOCAM is very sensitive to strongly starforming galaxies at 14.3 μm (Väisänen et al. 2002) and based on ELAIS counts about 6 galaxies are expected in a region of this size at the achieved sensitivity.

Also, many of our ISOCAM sources are only detected at 14.3 μm (16 sources; see Table 2) but since only about 6 galaxies are statistically expected in the region starburst galaxies can only account for some of these sources, most likely the faint ones due to the steep luminosity function and red colours of such galaxies. Our source detection limits at 6.7 μm and K are about 12.5 and 17.5 mag. respectively. Yet many of the sources seen only at 14.3 μm are very bright (e.g. ISO-L1551-

51; $m_{14.3} = 7.96$) indicating that these sources are most likely asteroids. In fact, no starburst galaxies brighter than about $F_{14.3} \sim 5$ mJy are expected in the whole region and the motion of asteroids would explain why these bright sources are only detected in one filter. Given the proximity of L1551 to the ecliptic plane and the large number of asteroids with orbits in this region this seems very likely.

There are numerous known Herbig-Haro objects in the observed region. These shock-excited emission line nebulae are associated with outflows from protostellar sources and radiate mainly in H recombination lines and forbidden lines such as [S II]($\lambda\lambda$6717, 6732), see e.g. HST observations of HH 29 (Devine et al. 2000). At infrared wavelengths we could also expect line emission through H_2 rovibrational lines and in the ISOCAM filters used for our observations we especially have 5 pure rotational H_2 lines (H_2 0-0 S(4) through S(8)) in the 6.7 μm filter and 2 pure rotational lines (S(1) and S(2)) in the 14.3 μm filter. As can be seen in Fig. 8 the very bright Herbig-Haro objects HH 28 and HH 29 have 6.7 μm peaks that are clearly separated from the corresponding Hα peaks. Since the mid-IR and Hα traces very different conditions this could be expected, however, there is also the possibility that extended YSO candidates in fact are galaxies seen through the dark molecular cloud. As with galaxies, Herbig-Haro objects cannot be easily separated from YSOs using only the $m_{6.7} - m_{14.3}$ colour. Deep imaging or spectra of the new YSO candidates is needed to confirm their nature. Deep images, preferably in the IR (much deeper than our K images), could show if the YSO candidates look extended or point source like. Also, one
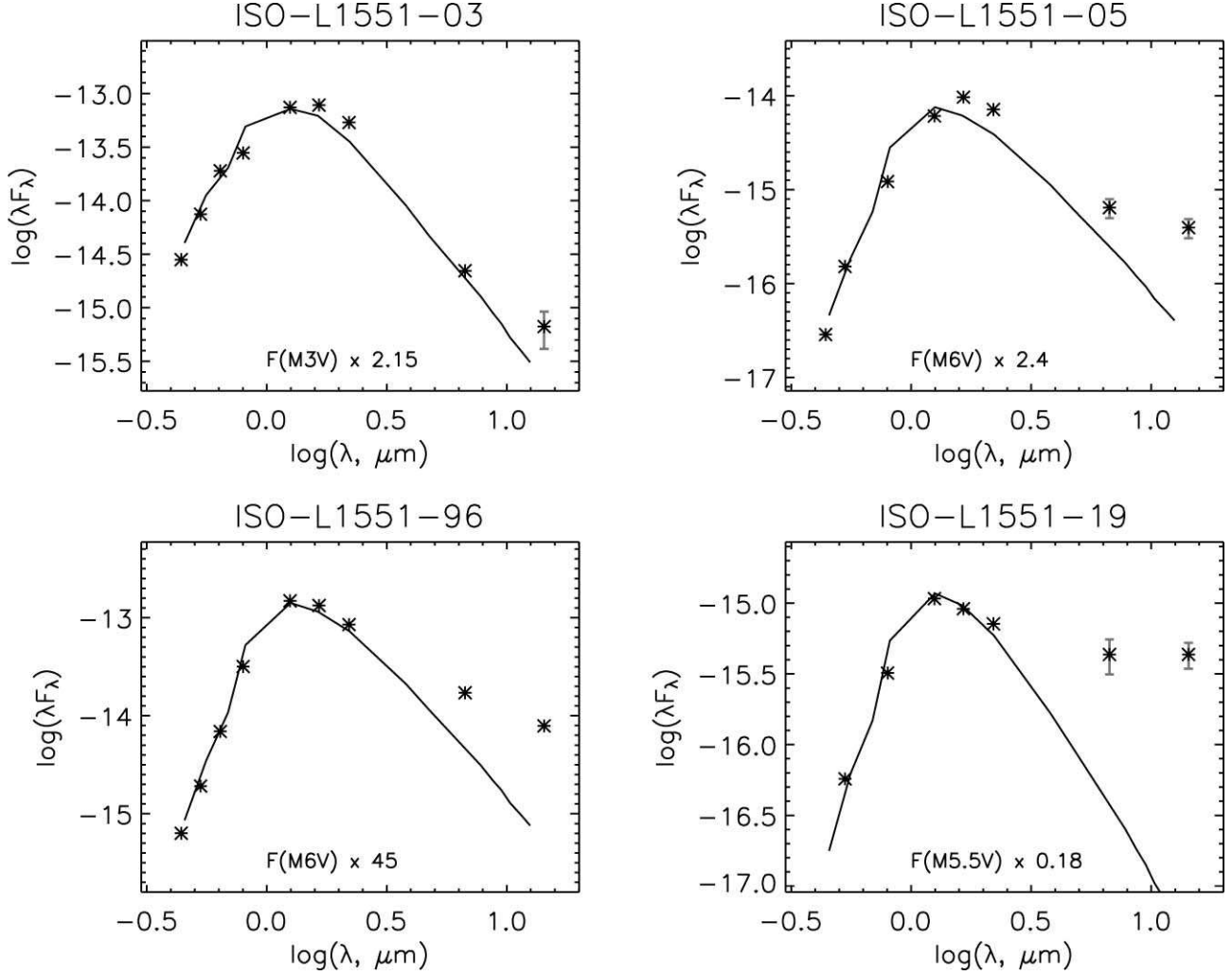
Fig. 5. The SEDs of four 'red' ISOCAM sources compared to scaled SEDs of M dwarfs. In each case an IR excess is clearly seen.

could compare an image taken through an [S II] interference filter (where HH objects are strong) with a broadband image centred at about 1 micron (where HH objects are weak). Spectra of the YSO candidates could be used to search for strong Hα emission and Li I λ6707 in absorption which would indicate a T Tauri star.

In Figure 7, images are shown for most of the YSO candidates visible in our *I* or *K*-band observations. Both ISO-L1551-10 and 72 are easily seen in the optical/near-IR but are not included since they are single point sources well within the ISOCAM error circle. Several of the YSO candidates are extended in a spherical or elliptical manner, supporting that these might be galaxies seen through the dark cloud.

At least three of the observed ISOCAM sources have known spectral types from previous studies. ISO-L1551-47 (HD 285845) is a binary system with a separation of 73 mas (Schneider et al. 1998), excluded from cloud membership by its radial velocity and proper motion (Walter et al. 1988). The primary component is of spectral type G8 and has colour indices consistent with that of a main sequence star (Walter et al. 1988). Its distance is implied to be 90 pc from its photometric parallax and it is a bright X-ray source (Favata et al. 2003).

This suggests that ISO-L1551-47 is an active binary system in the foreground of L1551.

ISO-L1551-44 (MHO 4, Briceño et al. 1998) and ISO-L1551-96 (MHO 5) are known to be very similar YSOs, both very late type TTS of spectral type M6–6.5. They have strong Li I λ6707 in absorption and Hα in emission and similar ages ∼ 1 Myr and masses ∼ 0.05 $M_\odot$, placing them in the brown dwarf region. Both were detected at 6.7 and 14.3 μm, but only ISO-L1551-96 has mid-IR excess at 14.3 μm. ISO-L1551-44, however, shows no mid-IR excess at 6.7 μm nor in the *K*-band, and is therefore a very late type NTTS.

ISO-L1551-21 has previously been detected in X-ray observations (L1551 X13, Carknet et al. 1996) where it was suggested to be unrelated to the cloud since it was identified with LP 415-1165, a foreground dM star appearing in the Luyten (1971) proper motion catalogue. It lies close to the Herbig-Haro objects HH 28 (17″ E) and HH 258 (20″ NW) but is definitely a point source.

ISO-L1551-61 (HH 30) is a very well known YSO, observed as an optically thick circumstellar disk seen edge on. HST observations (Burrows et al. 1996) have shown clearly that this star is not observed directly, only nebulosity is seen.

ISO-L1551-65 lies at the position of a known triple radio continuum source, probably extragalactic in nature (Rodríguez & Cantó 1983) with an overall extent of $\sim 20''$. It is however unclear if this is the object detected with ISOCAM.

The SEDs for three of the new YSO candidates (ISO-L1551-3, 5, 19) and the known YSO MHO 5 (ISO-L1551-96) are shown in Fig. 5. These sources have at least 7 known broad band magnitudes (see Table 2), making it worthwile to plot their SEDs. No extinction corrections have been applied for the new candidates (since no spectral classes are known), however, they are all outer members of L1551, located quite far away from the dense central region so the extinction is probably not that large (especially for ISO-L1551-3, see Fig. 1). For MHO 5 the extinction is known to be only $A_V = 0.01$ (Briceño et al. 1998) locating it on our side of the cloud with a negligible extinction. For each source a spectral class has been calculated by fitting the observed SEDs with scaled SEDs of M dwarfs as given by Leggett (1992). The known brown dwarf MHO 5 (ISO-L1551-96) is very well fitted using a M6 dwarf, this agrees with the spectral type M6–6.5 found from spectra of this source (Briceño et al. 1998). The three YSO candidates have SEDs that mimics dwarfs of spectral types M3, M6 and M5.5 respectively. All four sources show mid-IR excess when compared to the scaled SEDs. For ISO-L1551-3 the excess is small and only at $14.3\,\mu m$ which could indicate that the inner part of its accretion disk has been cleared out while the excess originates further out where the dust is cooler.

5. Conclusions

Based on a deep mid-IR ISOCAM survey (approximately $20' \times 20'$) of the L1551 dark molecular cloud we have found 14 sources with intrinsic mid-IR excess emission at $14.3\,\mu m$ which were therefore classified as YSO candidates. Additional observations in B, V, I, J, H and K supported the YSO candidate status for most detected candidates and yielded three more candidates. Out of the 17 detected YSO candidates only two were previously known (HH 30 and MHO 5). This means 15 new candidates, however, several of these are extended and could be background galaxies or Herbig-Haro objects. Assuming a co-eval age of 2-3 Myr for our sample (mainly Class II objects) and that all candidates actually are YSOs we only add a few solar masses to the stellar mass component of the Star Formation Efficiency (SFE) in L1551. This is however a small contribution when compared to the previously known YSO population. The new YSO candidates add to the low-mass end of the IMF in L1551, but due to the small number of known YSOs (as expected since L1551 has a mass of only $\sim 80\,M_\odot$, Snell 1981) and the lack of follow-up spectra, the IMF can not be accurately modelled yet. In addition to the 5 known outflow YSOs (HH 30, HL/XZ Tau, L1551 IRS 5 and L1551 NE) two brown dwarfs were previously known in the region and one of these, MHO 5, belongs to the ISOCAM YSO candidates and was found in our study to have mid-IR excesses compatible with being in a Class II phase of evolution. Most of the YSO candidates, assuming they are real, seem to belong to the YSO class II group (Classical T Tauri Stars) and thus have optically thick circumstellar disks at mid-IR wavelengths. One of the sources (ISO-L1551-61 = HH 30) has even been seen as an optically thick edge-on disk with the HST. Obviously, more follow-up studies from the ground should be made, especially spectroscopic observations of all the new YSO candidates which is necessary to confirm their YSO status since some of them could well be background galaxies seen through the dark molecular cloud or Herbig Haro objects caused by the known YSOs with outflows, close to the centre of L1551.

References

André P., Montmerle T., 1994, ApJ 420, 837
André P., Ward-Thompson D., Barsony M., 1993, ApJ 406, 122
Biviano A., Sauvage M., Gallais P., et al., 2000, Experimental Astronomy, v. 10, Issue 2/3, p. 255-277
Bontemps S., Andr P., Kaas A.A., et al., 2001, A&A 372, 173
Briceño C., Hartmann L., Stauffer J., et al., 1998, AJ 115, 2074
Burrows C.J., Stapelfeldt K.R., Watson A.M., et al., 1996, ApJ 473, 437
Carkner L., Feigelson E.D., Koyama K., et al., 1996, ApJ 464, 286
Coulais A., Abergel A., 2000, A&AS 141, 533
Dale D.A., Silbermann N.A., Helou G., et al., 2000, AJ 120, 583
Delaney M.(ed.), 2000, ISOCAM Interactive Analysis User's Manual, Version 4.0, ESA Document, Reference Number SAI/96-5226/Dc
Devine D., Reipurth B., Bally J., 1999, AJ 118, 972
Devine D., Bally J., Reipurth B., et al., 2000, ApJ 540, L57
Emerson J.P., Harris S., Jennings R.E., 1984, ApJ 278, L49
Favata F., Giardino G., Micela G., et al., 2003, A&A 403, 187
Fridlund M., White G.J., 1989a, In: Winnewisser G.(ed.) Physics and Chemistry of Molecular Clouds. p.198
Fridlund M., White G.J., 1989b, A&A 223, L13
Garnavich P.M., Noriega-Crespo A., Green P.J., 1992, RMxAA 24, 99
Giovanardi C., Rodríguez L.F., Lizano S., et al., 2000, ApJ 538, 728
Gomez M., Jones B.F., Hartmann L., et al., 1992, AJ 104, 762
Graham J.A., Heyer M.H., 1990, PASP 102, 972
Kaas A.A., Olofsson G., Bontemps S., et al., 1999, in: The Universe as Seen by ISO. Eds. P.Cox & M.F.Kessler. ESA-SP 427
Kenyon S.J., Dobrzycka D., Hartmann L., 1994, AJ 108, 1872
Lada C.J. & Wilking B.A., 1984, ApJ 287, 610
Lada C.J., 1987, In: IAU Symp. 115, Star Forming Regions, eds. Peimbert M. & Jugaku J., p.1
Leggett S.K., 1992, ApJS 82, 351
Looney L.W., Mundy L.G., Welch W.J., ApJ 484, L157
Luyten W.J., 1971, The Hyades (Minneapolis: Univ. of Minnesota)
Lynds B.T., 1962, ApJS 7, 1
Minn Y.K., 1991, JKAS 24,191
Miville-Deschênes M.A., Boulanger F., Abergel A., et al., ISO Beyond Point Sources: Studies of Extended Infrared Emission, September 14-17, 1999, ISO Data Centre, Villafranca del Castillo, Madrid, Spain. Edited by R.J.Laureijs, K.Leech and M.F. Kessler, ESA-SP455, 2000. p.27.

Moriarty-Schieven G.H., Powers J.A., Butner H.M., et al., 2000, ApJ 533, L143

Olofsson G., Huldtgren M., Kaas A.A., et al., 1999, A&A 350, 883

Osorio M., D'Alessio P., Muzerolle J., et al., 2003, ApJ 586, 1148

Ott S., Abergel A., Altieri B., et al., 1997, In: Hunt G., Payne H.E. (eds.) Astronomical Data Analysis Software and Systems. ASP Conf. Ser. 125, 34

Parker N.D., White G.J., Hayashi S.S., et al., 1991, A&A 250, 134

Persi P., Marenzi A.R., Olofsson G., et al., 2000, A&A 357, 219

Rainey R., White G.J., Richardson K.J., et al., 1987, A&A 170, 237

Reipurth B., 2000, AJ 120, 3177

Rodríguez L.F., Cantó J., 1983, Rev. Mexicana Astron. Astrofis. Ser. Conf. 8, 163

Schneider G., Hershey J.L., Wenz M.T., 1998, PASP 110, 1012

Snell R.L., Loren R.B., Plambeck R.L., 1980, ApJ 239, L17

Snell R.L., 1981, ApJS 45, 121

Starck J.L., Murtagh F., Pirenne B., Albrecht M., 1996, PASP 108, 446

Strom K.M., Strom S.E., Vrba F.J., 1976, AJ 81, 320

Väisänen P., Morel T., Rowan-Robinson M., et al., 2002, MNRAS 337, 1043

Wainscoat R.J., Cohen M., Volk K., et al., 1992, ApJS 83, 111

Walter F.M., Brown A., Mathieu R.D., et al., 1988, AJ 96, 297

White G.J., Liseau R., Men'shchikov A.B., et al., 2000, A&A 364, 741

Fig. 6. Final 6.7 μm ISOCAM map, the image shown is approximately $10' \times 20'$. Point sources are marked with circles, while squares indicate extended sources (the pixel size is $6''$). Plus signs mark the positions of L1551 NE, L1551 IRS5, HL and XZ Tau.
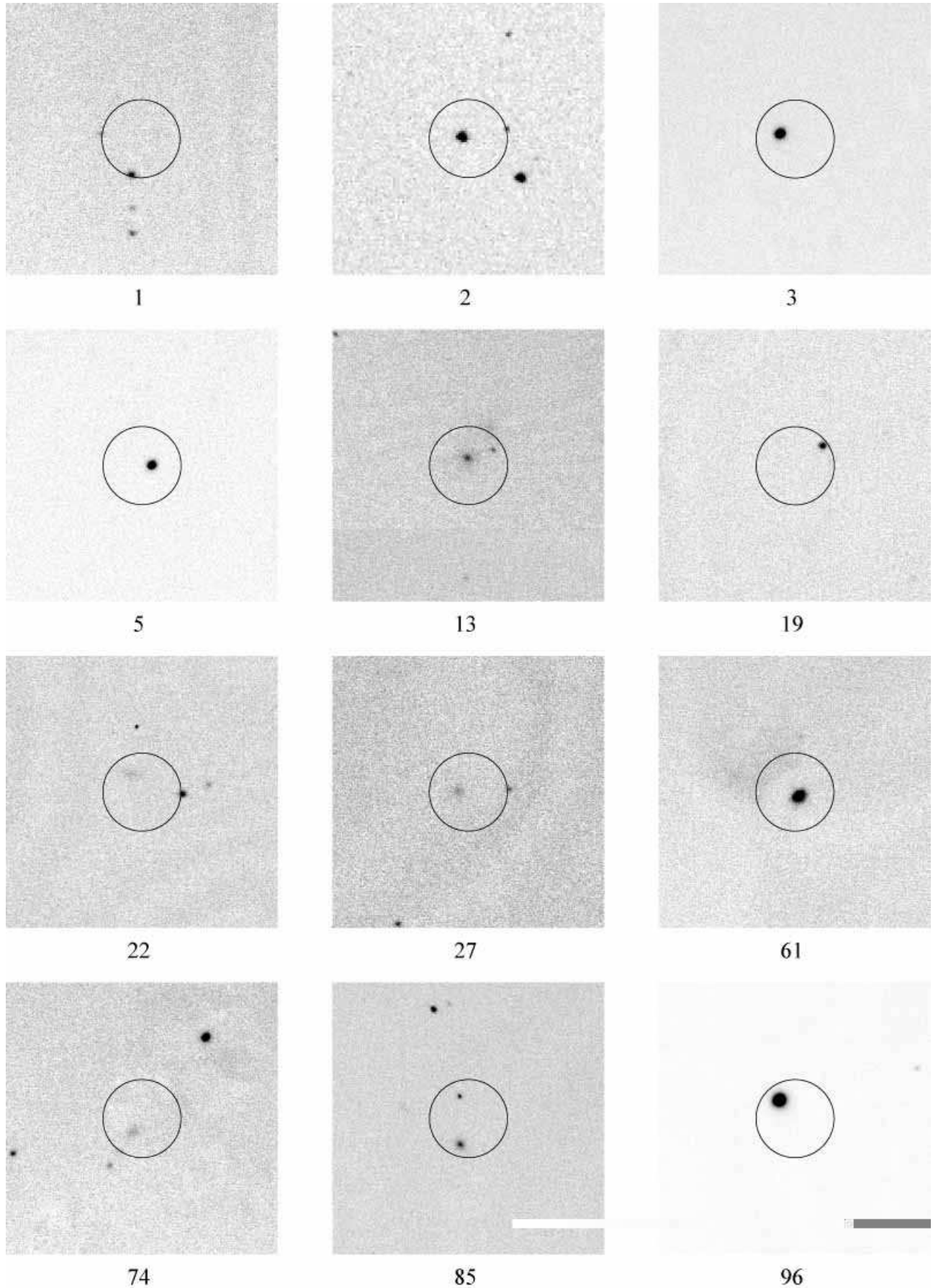
Fig. 7. *I*-band images (except for ISO-L1551-2, *K*-band image). All images show a 1′ × 1′ field centred on ISOCAM source coordinates where the position uncertainty is indicated with 8″5 radius error circles. ISO-L1551-1 and ISO-L1551-85 are both double in the *I*-band images, however, it is probably the south component that has an mid-IR excess in both cases.

Fig. 8. Hα mosaic of L1551 observed with the 2.56 m NOT telescope (exposure time 1200 s). The contours represent levels of constant flux in the ISOCAM 6.7 μm map. Hα image kindly provided by M. Fridlund.

Table 2. All ISOCAM sources in L1551, with additional optical & near-IR photometry.

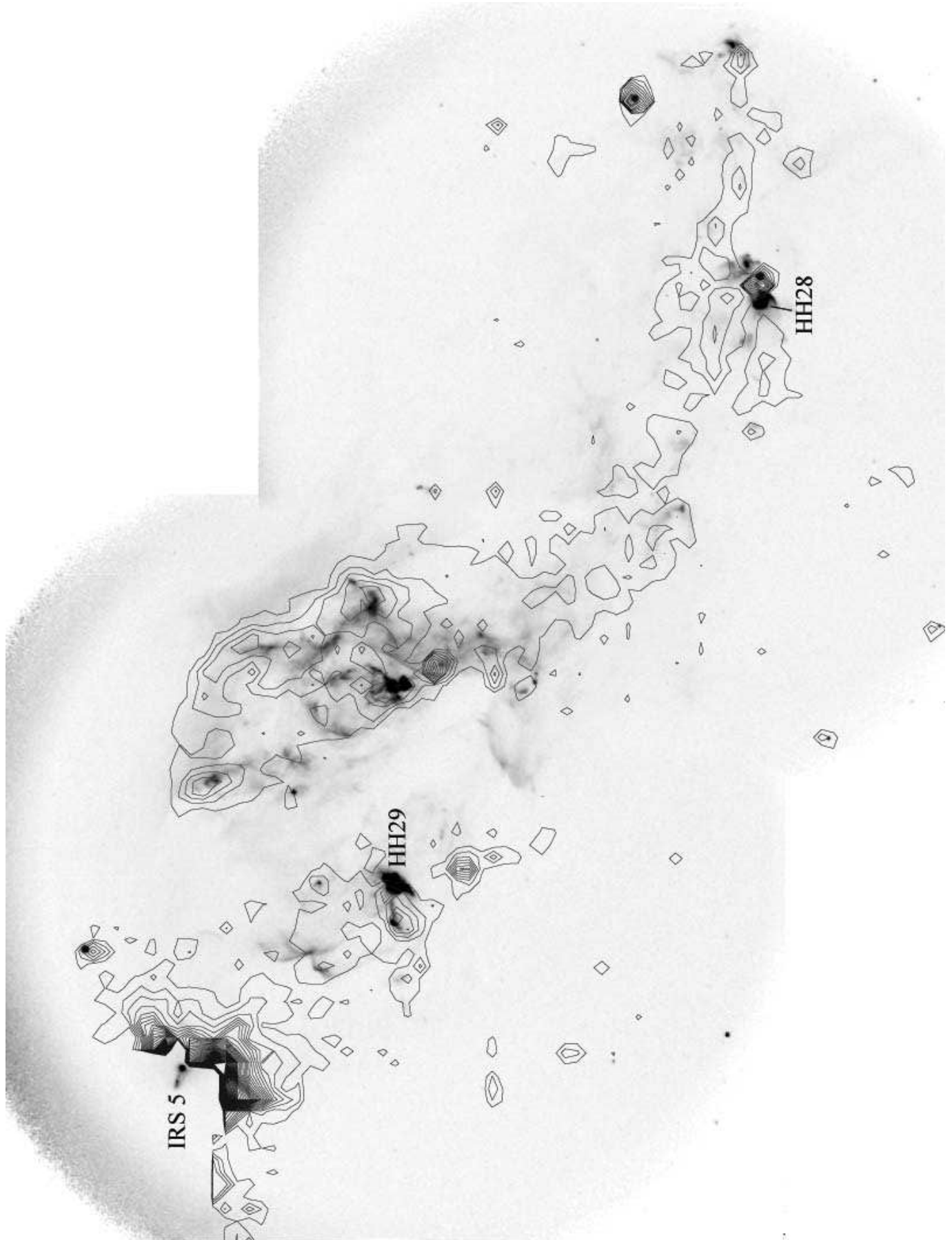| ISO-L1551	RA(2000)	DEC(2000)	$F_{6.7}$	$F_{14.3}$	B	V	R	I	J	H	K_S	6.7 μm	14.3 μm	Remarks
1	04:30:43.1	17:58:30	1.56			22.27		19.07	16.89	16.02	15.94	11.81		Sep 8″2 S
								20.56						Sep 9″2 E
2	04:30:43.7	17:54:25	0.79:	0.97:	15.9[d]	out	14.5	out	12.87	12.43	12.23	12.56:	10.72:	
3	04:30:48.4	18:18:36	4.95	3.18	17.58	16.10	14.7	13.84	11.82	10.97	10.56	10.56	09.44	
4	04:30:50.0	18:05:20	1.87		20.96	18.94		15.99	13.38	12.32	11.75	11.62		
5	04:30:50.9	18:13:00	1.44	1.88	22.56	20.33		17.24	14.54	13.24	12.75	11.90	10.01	
6	04:30:51.7	18:10:23	0.91			21.06		17.83	15.05	13.73	13.25	12.40		
7	04:30:52.1	17:59:00	2.55		21.19	19.83		18.21			15.92[e]	11.28		
8	04:30:52.8	18:18:19	1.12			20.01		16.88	14.12	12.81	12.24	12.17		
9	04:30:53.3	17:53:37	3.99		16.61	15.22	14.0	13.36	11.97	11.28	11.06	10.80		
10	04:30:53.8	17:59:09	2.00		22.62	20.74		17.50	15.43	14.52	14.18	11.55		near HH 256
11	04:30:54.2	17:58:24	17.96	2.55	16.72	sat	13.1	12.40	10.55	09.60	09.34	09.16	09.68	GSC1269:485
12	04:30:54.6	17:55:16	19.16	2.21	12.3[d]	sat	11.0	10.47	09.59	09.31	09.17	09.09	09.83	GSC1269:261
13	04:30:58.2	18:03:29	1.76	2.47		21.76		18.97	16.97	15.85	15.17	11.69	09.71	Galaxy ?
14	04:30:59.4	18:01:24		2.78										09.58	
15	04:30:59.8	18:04:25	8.01	1.84	17.96	16.16	14.7	13.71	11.61	10.66	10.28	10.04	10.03	
16	04:30:59.8	17:59:56	3.74		17.25	15.66	14.2	13.59	12.04	11.28	10.97	10.87		
17	04:31:00.2	18:03:45		0.99	22.59	21.41		18.78	16.69	15.82	15.48		10.70	Sep. 8″9 ESE
					23.17			20.26						Sep. 3″6 ESE
18	04:31:01.2	18:18:23	2.00		21.07	18.93		16.03	13.67	12.50	11.99	11.55		
19	04:31:01.8	18:03:00	0.97	2.07		21.39		18.69	16.42	15.80	15.25	12.33	09.90	
20	04:31:05.7	18:14:12	1.62						18.71	16.04	13.92	11.77		
21	04:31:05.8	18:03:19	4.79		17.43	15.94	15.0	13.26	11.69	11.10	10.84	10.60		L1551 X13[a]
22	04:31:05.9	18:01:48	0.95	1.52				19.72			14.93[e]	12.35	10.24	Galaxy ?
23	04:31:07.2	18:14:33	0.82						17.68	15.19	13.66	12.52		
24	04:31:08.2	18:08:12	1.18					19.22	15.53	14.04	13.29	12.12		
25	04:31:08.7	18:18:37		4.94									08.96	
26	04:31:08.9	18:19:02	1.59		19.63	17.84	16.6	15.18	13.48	12.56	12.31	11.80		Double (1″8)
27	04:31:08.9	18:01:43	0.87	2.38				19.93			15.37[e]	12.45	09.75	Galaxy ?
28	04:31:09.0	18:03:44		1.51							17.7[e]		10.24	
29	04:31:11.2	18:11:05	0.80						16.90	14.65	13.38	12.54		
30	04:31:11.9	18:08:18	0.73									12.64		
31	04:31:12.5	18:17:49		4.21									09.13	
(32)	04:31:14.1	18:10:22		0.63									11.20	
33	04:31:15.9	18:09:15	5.72	0.75		22.61		18.07	13.88	12.15	11.29	10.41	11.01	
34	04:31:16.3	18:18:34	6.10		14.3[d]	sat	12.5	12.37	11.24	10.65	10.45	10.34		GSC1269:1201
35	04:31:17.6	18:06:24		1.82									10.04	HH 264 ?
36	04:31:17.6	18:01:53	1.06		22.36	20.06		16.78	14.08	12.94	12.42	12.23		
37	04:31:19.0	18:03:02		0.93							16.86[e]		10.77	
38	04:31:19.3	18:09:21	1.30					20.25	15.75	13.75	12.75	12.02		Close double ?
39	04:31:20.2	18:01:45	2.06		19.79	18.05	16.9	15.41	13.19	12.24	11.83	11.52		
40	04:31:21.2	17:59:49	0.62	1.03								12.82	10.66	X-ray source[f]
41	04:31:21.6	18:02:50	1.25		22.00	19.92		16.63	14.07	12.83	12.31	12.05		
42	04:31:22.5	18:14:51	0.75			17.10	15.9	15.13	13.56	12.67	12.44	12.61		
43	04:31:23.5	17:58:52	65.63	12.87	14.1[d]	sat	11.4	10.96	09.09	08.18	07.88	07.76	07.92	GSC1269:1017
44	04:31:24.3	18:00:25	8.53	1.27	20.38	18.67		14.50	11.65	10.92	10.57	9.97	10.43	MHO 4[b], X15[a]
45	04:31:24.6	18:13:30	0.85		18.44	16.98	15.9	15.05	13.49	12.78	12.50	12.47		Sep. 2″7 ENE
								21.95		20.15				Sep. 2″3 WSW
46	04:31:25.3	18:10:43	0.76									12.60		
47	04:31:25.5	18:16:19	48.56	7.62	11.0[d]	sat	09.9	sat	08.67	08.24	08.10	08.08	08.49	HD 285845
48	04:31:25.6	18:17:02	0.44		19.92	18.21	17.2	15.55	13.99	13.36	13.11	13.20		
49	04:31:26.3	18:05:52	4.25			21.98		18.28	14.75	13.30	12.58	10.73		Sep. 3″3 W
						22.39	20.60		17.03	13.79	12.46	11.74			Sep. 5″3 SE
50	04:31:26.6	18:06:59	1.40									11.93		HH 260 ?
51	04:31:27.0	18:10:41		12.30									07.96	
52	04:31:27.7	18:06:19	3.86									10.83		HH 29 ?
53	04:31:29.0	18:17:45		4.23									09.12	
(54)	04:31:29.1	18:18:16		1.29									10.42	
55	04:31:29.3	18:08:51	3.11		17.52	16.06	15.0	13.69	12.36	11.73	11.49	11.07		
(56)	04:31:29.9	18:06:10	1.01									12.29		
(57)	04:31:32.1	18:02:49	0.74									12.63		
58	04:31:33.4	18:04:57		1.24							16.71[e]		10.46	
59	04:31:34.0	18:05:34	1.32			23.24:		19.39	15.24	13.40	12.52	12.00		
(60)	04:31:35.2	18:01:54		0.58									11.27	
61	04:31:37.5	18:12:26	0.89	1.77	19.78	18.88	16.4	17.06	15.18	14.24	13.37	12.43	10.07	HH 30
62	04:31:37.6	18:02:58	1.67		19.90	18.14	17.2	15.72	13.73	12.66	12.34	11.75		
63	04:31:39.0	18:02:36	2.26		17.33	15.99	15.1	14.03	12.32	11.65	11.34	11.42		
(64)	04:31:40.7	18:09:03	2.36									11.37		
65	04:31:44.1	18:10:37	0.62	0.66							17.8[e]	12.82	11.15	VLA 21cm-15[c g]
(66)	04:31:44.2	18:12:38		1.07									10.62	
67	04:31:45.0	18:06:12		2.82									09.57	
68	04:31:45.3	18:14:37	11.08		17.55	16.28	15.1	14.13	11.86	10.67	10.06	09.69		
69	04:31:46.5	18:06:40		0.84									10.88	
70	04:31:55.7	18:11:00	1.60		20.18	18.33	17.0	15.27	13.31	12.45	12.12	11.79		
71	04:31:56.1	18:08:55	21.28	3.39	17.08	15.13	13.9	12.70	10.63	09.54	09.18	08.98	09.37	
72	04:31:56.4	18:13:36	0.87		20.82	19.48	19.1	17.60	16.21	15.26	15.09	12.45		
73	04:31:56.6	18:02:52	10.02	1.68	16.42	15.11	13.6	12.96	11.23	10.34	10.07	09.80	10.13	GSC1269:559
74	04:31:57.2	18:17:21	1.63	1.78		20.50		18.69			15.73[e]	11.77	10.06	Galaxy ?
75	04:31:57.6	18:11:21	1.81									11.66		
76	04:31:58.9	18:12:01	4.29								14.97[e]	10.72		
77	04:31:59.1	18:02:52	0.85		17.43	16.46	15.7	14.70	13.31	12.69	12.47	12.48		

Continued on next page...

Table 2. – continued from previous page

ISO-L1551	RA(2000)	DEC(2000)	$F_{6.7}$	$F_{14.3}$	B	V	R	I	J	H	K_S	6.7 μm	14.3 μm	Remarks
78	04:31:59.4	18:10:37	0.60		17.00	15.91	15.4	14.51	13.36	12.90	12.73	12.85		
79	04:31:59.5	18:13:49		6.67	21.33	20.10	19.2	18.47					08.63	Sep. 11″ N
						22.87		19.90						Sep. 14″ NNW
80	04:31:59.9	18:08:50	2.00		15.51	sat	13.9	13.25	12.13	11.67	11.48	11.55		GSC1269:777
81	04:32:00.6	18:12:09	2.69									11.23		
82	04:32:01.0	18:03:55		1.48									10.26	
83	04:32:01.1	18:12:33	2.42									11.34		HH / Galaxy ?
84	04:32:01.1	18:06:01	1.25		20.25	18.42	17.4	15.86	13.63	12.50	12.11	12.06		
85	04:32:01.1	18:05:07	0.61	1.34	22.39	20.91		18.88	16.63	15.49	15.05	12.84	10.37	Sep. 6″0 SSE[h]
						22.91		19.86						Sep. 5″3 NNE
86	04:32:01.3	18:11:29	3.24	3.86								11.02	09.22	HH 262 ?
87	04:32:01.5	18:11:59		2.22									09.83	HH object ?
88	04:32:02.6	18:03:15	0.55		17.44	16.18	15.2	14.72	13.52	12.99	12.79	12.94		
89	04:32:03.6	18:06:06	25.93	6.57	17.15	15.14	13.5	12.51	10.26	09.11	08.68	08.77	08.65	GSC1270:357
90	04:32:07.2	18:14:28	0.41		17.70	16.39	15.4	14.74	13.45	12.75	12.57	13.28		
91	04:32:07.4	18:16:28	4.54		16.24	sat	13.7	13.05	11.64	10.84	10.62	10.66		GSC1270:1234
92	04:32:07.4	18:09:05	0.82		16.54	15.55	14.7	14.20	13.07	12.60	12.44	12.51		
93	04:32:09.5	18:12:02	1.67									11.74		HH / Galaxy ?
94	04:32:10.9	18:17:41	3.26		14.0[d]	sat	12.8	12.54	11.63	11.29	11.13	11.02		GSC1270:401
(95)	04:32:13.4	18:17:51		0.80									10.93	
96	04:32:15.8	18:12:43	38.34	37.55	19.20	17.58	15.8	13.70	11.07	10.39	10.06	08.34	06.75	MHO 5[b]

[a] Carkner et al. 1996
[b] Briceño et al. 1998
[c] Giovanardi et al. 2000 – Could be an extragalactic triple radio source (Rodríguez & Cantó 1983)
[d] USNO A-2 catalogue has been used
[e] K-band magnitude (ARNICA/NOT)
[f] XMM-Newton-15, Favata et al. 2003
[g] XMM-Newton-35
[h] XMM-Newton-49